

Cosmic evolution of bars in simulations of galaxy formation

Takashi OKAMOTO¹

¹*Department of Cosmosciences, Graduate School of Science, Hokkaido University, N10 W8, Kitaku, Sapporo, 060-0810, Japan
okamoto@astro1.sci.hokudai.ac.jp*

Mari ISOE^{2,3}

²*Department of Astronomy, School of Science, The University of Tokyo, 7-3-1 Hongo, Bunkyo-ku, Tokyo 113-0033*

³*Division of Theoretical Astronomy, National Astronomical Observatory of Japan, 2-21-1 Osawa, Mitaka, Tokyo 181-8588
isoe.mari@nao.ac.jp*

and

Asao HABA¹

habe@astro1.sci.hokudai.ac.jp

(Received ; accepted)

Abstract

We investigate the evolution of two bars formed in fully self-consistent hydrodynamical simulations of the formation of Milky Way-mass galaxies. One galaxy shows higher central mass concentration and has a longer and stronger bar than the other at $z = 0$. The stronger bar evolves by transferring its angular momentum mainly to the dark halo. Consequently the rotation speed of the bar decreases with time, while the amplitude of the bar increases with time. While these features qualitatively agree with the results obtained by idealized simulations, our bars show some unusual behaviors. The pattern speed of the stronger bar largely goes up and down within a half revolution in its early evolutionary stage. This unsteady rotation occurs when the bar is misaligned with the $m = 4$ mode Fourier component. The amplitude of the weaker bar does not increase despite the fact that its rotation slows down with time. This result contradicts what is expected from idealized simulations and is caused by the decline of the central density associated with the mass loss and feedback from the stellar populations. In both galaxies, the bars are terminated around $4(\Omega - \Omega_{\text{bar}}) = \kappa$ resonances, where Ω , Ω_{bar} , and κ are, respectively, the angular frequency of a circular orbit, the bar patten speed, and the radial angular frequency.

Key words: cosmology: theory – galaxies: formation – galaxies: evolution – galaxies: structure–methods: numerical

1. Introduction

Bars are ubiquitous in the nearby disk galaxies (Eskridge et al. 2000; Barazza et al. 2008) and the bar fraction seems to be a strong function of redshift; it decreases by a factor of three from $z = 0$ to $z = 0.8$ (Sheth et al. 2008). Bars can affect galaxy properties by driving secular evolution (Combes & Sanders 1981; Pfenniger & Norman 1990; Combes & Elmegreen 1993; Debattista et al. 2004; Athanassoula 2005), and thus a number of simulations have performed to study their formation and evolution processes.

Most of the simulations employ idealized initial conditions for isolated galaxies in order to answer specific questions (e.g. Combes et al. 1990; Debattista & Sellwood 2000; Athanassoula 2003; Martinez-Valpuesta et al. 2006). A general picture obtained by these studies is that a bar continuously grows and slows down with time as its angular momentum gets transfered to the dark halo and the outer disk (e.g. Weinberg 1985; Combes & Elmegreen 1993; Athanassoula 2003).

In reality however disks and dark halos keep growing while bars form and evolve. The dark halos resulting from cosmological simulations are naturally triaxial

(Frenk et al. 1988; Jing & Suto 2002) and abundant in sub-structure (Moore et al. 1999; Klypin et al. 1999; Springel et al. 2008), both of which should exert torque on bars. Galaxy interactions could trigger bar formation (Miwa & Noguchi 1998; Berentzen et al. 2004). Moreover, even disk orientation changes with time owing to the misalignment of the angular momentum vector of the newly accreting gas (Okamoto et al. 2005; Okamoto 2013).

Early attempts to investigate the effects of cosmological growth of galaxies on the bar evolution are made either by simplifying the initial density perturbations (Heller et al. 2007; Romano-Díaz et al. 2008) or by embedding a live disk in a growing dark halo (Curir et al. 2006). Kraljic et al. (2012) use a cosmological N -body simulation as boundary conditions for sticky particle simulations and follow galaxy and bar evolution in evolving halos. They confirm that the bar fraction in fact decreases with increasing redshift. Scannapieco & Athanassoula (2012) analyse the bars in fully self-consistent simulations of galaxy formation at $z = 0$ and compare their properties with those in the idealized simulations.

Only recently have cosmological simulations with sufficient resolution to follow evolution of detailed structure in disk galaxies become possible (Guedes et al.

2011; Okamoto 2013; Stinson et al. 2013; Marinacci et al. 2014). An important difference of these simulations from the idealized simulations is that they invoke much stronger stellar feedback than the idealized simulations normally assume, otherwise simulations form too many stars for a given halo mass (e.g. Scannapieco et al. 2012; Okamoto 2013; Okamoto et al. 2014). The feedback is so strong that it can lower the central stellar and dark matter density during the galaxy evolution (Duffy et al. 2010; Governato et al. 2012), and hence the resonance structure would be also altered.

Two Milky Way-mass galaxies formed in the cosmological simulations by Okamoto (2013) offer a unique opportunity to investigate the evolution of bars in the context of the Λ cold dark matter cosmology. One galaxy is clearly barred from $z \simeq 1$ to 0, while the other has a much weaker bar. In this paper we compare and contrast these two galaxies focusing on the evolution of their bars. We also compare their properties with those obtained by idealized simulations.

This paper is organized as follows. In section 2 we briefly describe the simulations and galaxies we analyze. We present our results in section 3. We then discuss them and summarize our main conclusion in section 4.

2. Sample galaxies

We study the evolution of the bars formed in two smoothed particle hydrodynamic (SPH) simulations of galaxy formation in a Λ CDM universe. The cosmological parameters employed in these simulations are: $\Omega_0 = 0.25$, $\Omega_\Lambda = 0.75$, $\Omega_b = 0.045$, $\sigma_8 = 0.9$, $n_s = 0.9$, and a Hubble constant of $H_0 = 100 h \text{ km s}^{-1} \text{ Mpc}^{-1}$, where $h = 0.73$. The galaxies are selected from a cosmological periodic box of a side length of $100 h^{-1} \text{ Mpc}$ and called ‘Aq-C’ and ‘Aq-D’ according to the labelling system of the Aquarius project (Springel et al. 2008).

The dark matter particle masses are 2.6×10^5 and $2.2 \times 10^5 M_\odot$ for Aq-C and Aq-D, respectively, and the original SPH particle masses are 5.8×10^4 and $4.8 \times 10^4 M_\odot$, respectively. At $z < 3$ the gravitational softening lengths are fixed in physical coordinates as $\epsilon = 0.257$ and 0.240 kpc respectively in Aq-C and Aq-D. The simulations include radiative cooling, photo-heating by the ultra-violet background (Okamoto et al. 2008), star formation, timed release of energy, mass, and metals by type II and Ia supernovae and AGB stars (Okamoto et al. 2010; Okamoto 2013).

The stellar masses of these galaxies at $z = 0$ are $4.0 \times 10^{10} M_\odot$ (Aq-C) and $3.1 \times 10^{10} M_\odot$ (Aq-D); hence their masses are close to that of the Milky Way. The global evolution and properties of these galaxies are fully described in Okamoto (2013). We here only show the evolution of the circular velocity profiles which is the most relevant to the current study.

As shown in figure 1, the central circular velocity continuously decreases with time in both galaxies. This is presumably due to the stellar mass loss and feedback since we do not find this behavior in simulations without stel-

lar mass loss or feedback. weaker feedback. This drop changes the resonance structure as we will show later. We also find that Aq-C has more centrally concentrated mass distribution than Aq-D. The vertical line indicates the radius inside which a baryonic component dominates as $v_c(r) < 1.1 \sqrt{GM_b(<r)}/r$, where G is the gravitational constant and $M_b(<r)$ is the total baryon mass (gas + stars) within the radius, r ; the disks are bar unstable when this condition is satisfied (Efstathiou et al. 1982), although this criterion is only appropriate for a pure N -body cold disk in a rigid halo (e.g. Athanassoula 2008). This radius is almost constant with redshift ($\simeq 1 \text{ kpc}$) in both galaxies. Similarly, the radius within which the baryon mass is equal to the dark matter mass is also constant with redshift ($\simeq 4 \text{ kpc}$), indicating that the stellar mass fractions as functions of radius do not evolve strongly.

3. Results

In this section, we first describe how we identify stellar bars in the simulated galaxies and then undertake a detailed study of the evolution of the bars in them. In the following analyses, the z -direction is chosen to be parallel to the angular momentum vector of stars within 5 per cent of the virial radius¹ at given redshift unless otherwise stated. Note that the disk orientation significantly changes with redshift (Okamoto et al. 2005; Okamoto 2013). We use stars with $|z| < 1 h^{-1} \text{ kpc}$ for computing the surface stellar density to avoid the contamination from the stars in the satellite galaxies.

3.1. Bar identification

The strength, length, and angle of a bar can be parameterized by the amplitude and phase of its Fourier component, defined by expressing the surface stellar density as a Fourier series,

$$\frac{\Sigma(r, \phi)}{\bar{\Sigma}(r)} = 1 + \sum_{m=1}^{\infty} A_m(r) \cos[m\{\phi - \phi_m(r)\}], \quad (1)$$

where $\Sigma(r, \phi)$ is the surface stellar density, ϕ is the azimuthal angle, $\bar{\Sigma}(r)$ is the azimuthally averaged surface stellar density at radius r , and A_m and ϕ_m are the amplitude and phase of the m -th Fourier component, respectively. This analysis is performed on a face-on projection.

Typically, the amplitude of the $m = 2$ mode, $A_2(r)$, has a peak if a bar exists. The phase, $\phi_2(r)$, should be constant in the bar region. We first identify the radius at which $A_2(r)$ takes the maximum value, A_2^{max} , and we call this radius r_2^{max} . The bar angle is defined as $\phi_{\text{bar}} = \phi_2(r_2^{\text{max}})$. We utilize the radial profile of the phase of the $m = 2$ Fourier component to determine the bar length. Outside the bar region, the phase should show large variation owing to a spiral structure or by the absence of clear structure. We thus define the bar length, r_{bar} , as the maximum radius where the bar angle ϕ_{bar} and the phase of the $m = 2$ component differ by less than

¹ The virial radius is calculated based on the spherical collapse model (Eke et al. 1996).

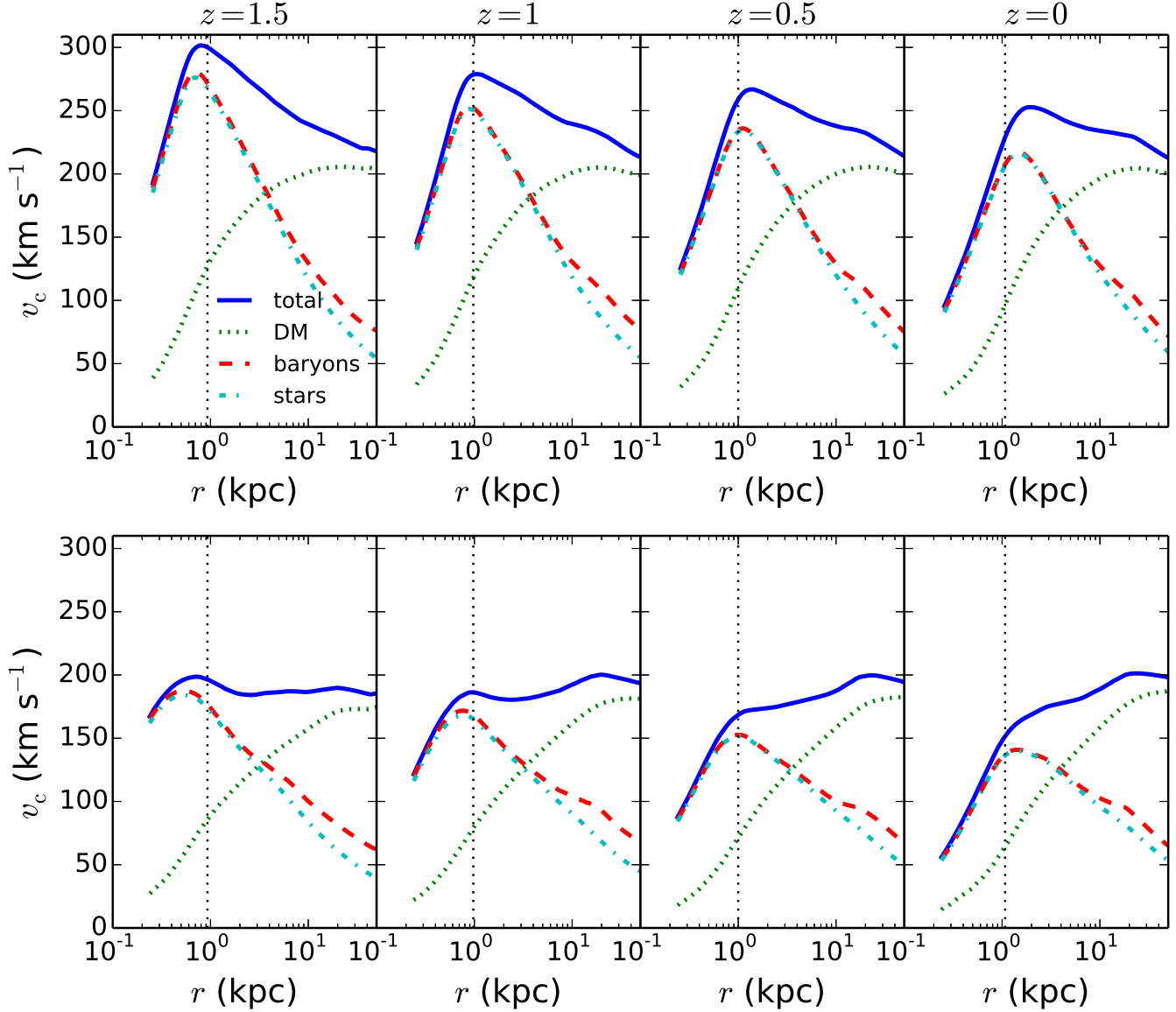


Fig. 1. Evolution of the circular velocity profiles. The upper and lower panels show Aq-C and Aq-D, respectively. From left to right, the circular velocities at $z=1.5$, 1.0, 0.5, and 0 are plotted as functions of radius. The blue solid lines are the circular velocities, $v_c(r) = \sqrt{GM(<r)}/r$, and the green dotted, red dashed, and cyan dot-dashed lines indicate the contribution of the dark matter, baryon, and stellar components, respectively. The vertical dotted lines indicate the radii at which $v_c(r) = 1.1 \sqrt{GM_b(<r)/r}$, where $M_b(<r)$ is the total baryon mass within the radius, r .

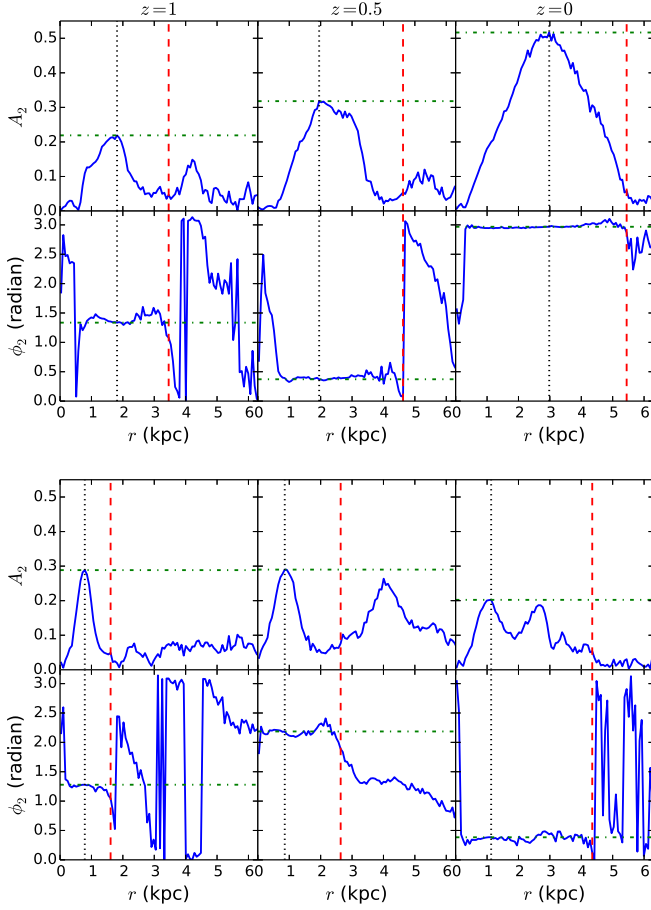


Fig. 2. The amplitude and phase profiles of the $m=2$ mode. The upper and lower six panels show Aq-C and Aq-D, respectively. From left to right, the results at $z=1, 0.5$, and 0 are presented. The bar length, r_{bar} , is indicated by the vertical red dashed line in each panel. The horizontal green dot-dashed lines indicate the values of A_2^{max} and ϕ_{bar} in the panels for amplitude and phase, respectively.

$\Delta\phi$. We employ $\Delta\phi = 0.1\pi$ in this paper. Scannapieco & Athanassoula (2012) find that this method yields consistent bar length with other methods which utilize the amplitude of the $m=2$ mode or the density profile along the bar².

We demonstrate this method in figure 2 where we plot the amplitude and phase profiles of the $m=2$ Fourier component at $z=1, 0.5$, and 0 . We find that the amplitude, $A_2(r)$, has a clear peak at each redshift and the phase, $\phi_2(r)$, is nicely constant around the peak. We hence conclude that both A_2^{max} and ϕ_{bar} are robustly defined by this method.

On the other hand, the bar length, r_{bar} , has weak dependence on the value of $\Delta\phi$ and thus it is less robustly defined. In most cases (5 out of 6 in figure 2), the bar lengths defined by the phase of the $m=2$ mode seem to be consistent with the behavior of the amplitude of the mode. In Aq-D however the amplitude, $A_2(r)$, has two peaks within the bar length at $z=0$. We have investi-

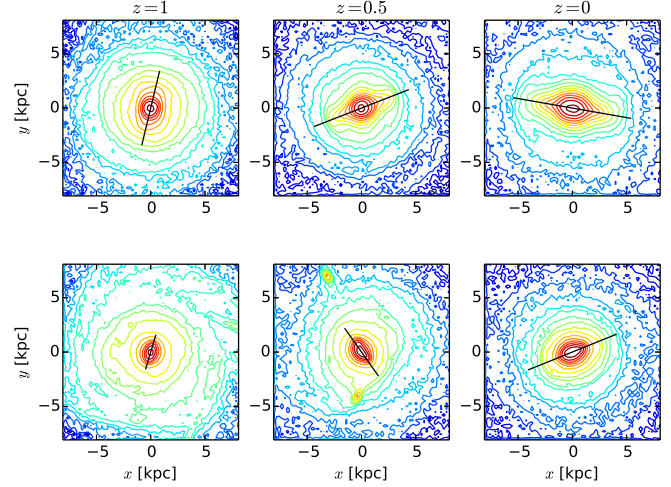


Fig. 3. Contour maps of the face-on stellar surface density of the galaxies. The upper and lower panels correspond to Aq-C and Aq-D, respectively, and the galaxies at $z=1, 0.5$, and 0 are shown from left to right. The contour levels are logarithmic. The black solid lines indicate the bars whose length and angle are defined as described in the text.

gated whether the outer peak is a different component from the inner peak, which is coincidentally aligned with the inner component. We find that the amplitude of the outer peak shows a rapid time variation and when it exists it aligns with the inner component. We thus hold our definition of the bar length throughout this paper. We will later show how the bar length changes if we exclude the outer component.

The bars identified this way are overplotted on the face-on surface stellar density maps in figure 3. The surface stellar density maps confirm that Aq-C always has a longer bar than Aq-D, while Aq-D has a better defined bar at $z=1$, which is evident from figure 2 where the value of A_2^{max} of Aq-D at $z=1$ is larger than that of Aq-C. We also find that Aq-D has more structure than Aq-C such as spiral arms and clumps. These clumps sink to the central region and add mass to the bulge (Okamoto 2013); thus it can change the bar properties by adding their angular momentum. By comparing the bar lengths and angles indicated by the straight lines in figure 3 with the shapes of the isodensity contours, we conclude that our method identifies the bars in the simulated galaxies well.

3.2. Redshift evolution

We now investigate the redshift evolution of the bars. We plot the bar lengths, r_{bar} , and the bar amplitudes, A_2^{max} , as functions of cosmic time and redshift in figure 4. We find that Aq-C's bar becomes longer and stronger with time. This behaviour is usually seen for bars in early-type disk galaxies (Combes & Elmegreen 1993) or bars in galaxies with centrally concentrated dark halos (Athanassoula 2003) in the idealized simulations. This is consistent with the fact that Aq-C has a massive bulge (Okamoto 2013) and its halo shows a high central concentration (figure 1).

Contrarily, Aq-D's bar does not show such strong evo-

² Scannapieco & Athanassoula (2012) employed $\Delta\phi = \arcsin(0.3)$.

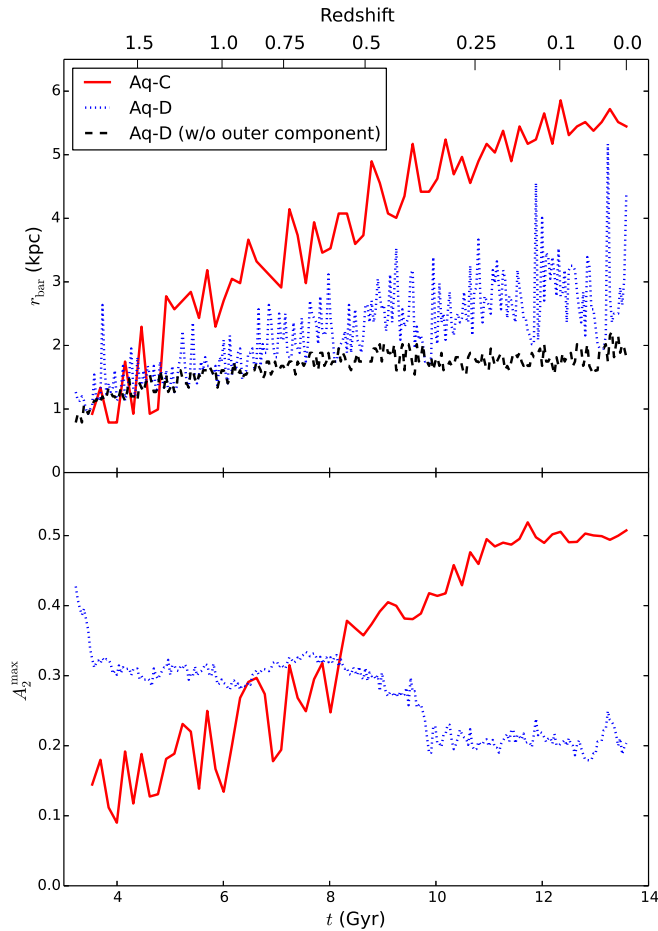


Fig. 4. Time evolution of the bar length, r_{bar} , and the amplitude, A_2^{max} . The upper panel shows the bar lengths as functions of time (or redshift). The red solid and blue dotted lines indicate Aq-C and Aq-D, respectively. The black dashed line represents the bar length of Aq-D when we exclude the outer component. The amplitude, A_2^{max} , is shown in the lower panel.

lution in the length and its amplitude is almost constant until $t \sim 9.8$ Gyr, at which it suddenly drops to the lower value. We also compute the bar length in Aq-D by excluding the component corresponding to the outer peak. To do so, we find the radius between the inner and outer peaks at which the amplitude, $A_2(r)$, takes the minimum value. If this radius is shorter than the bar length defined only by the phase profile, we employ this radius as the bar length. The bar length defined this way exhibits very weak time evolution. The comparison between two bar lengths with the different definitions indicates that the component corresponding to the outer peak varies violently with time.

3.3. Pattern speed of the bars

The time-steps used to output the simulation snapshots are too large to measure the bar pattern speed. Moreover, the change of the disk orientation with time (Okamoto 2013) makes it difficult to measure the pattern speed. We hence restart the simulations around $z = 1, 0.5$, and 0,

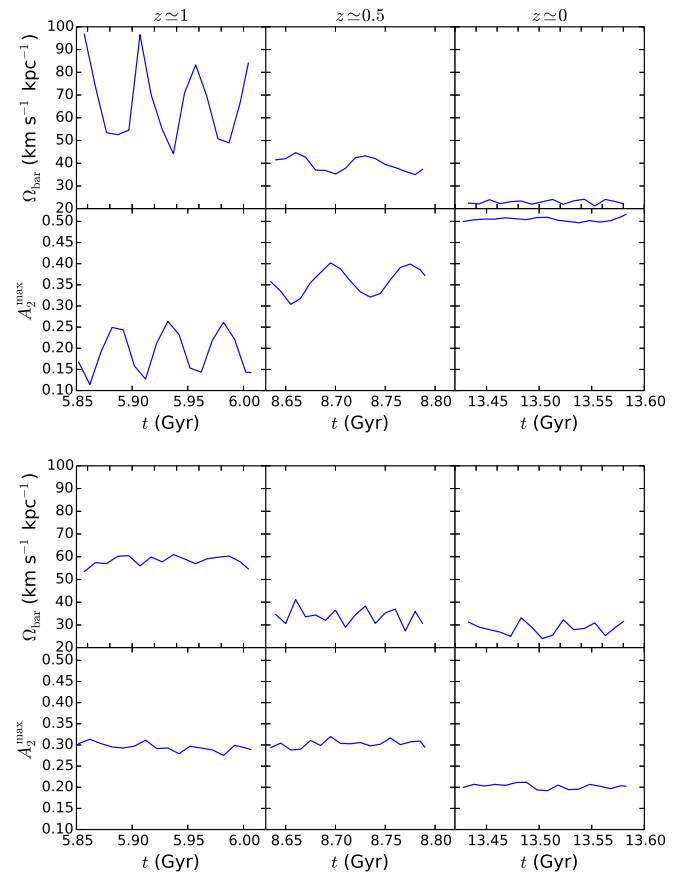


Fig. 5. Time evolution of the bar pattern speed, Ω_{bar} , and the amplitude, A_2^{max} , around $z = 1, 0.5$, and 0 (from left to right). We show Aq-C and Aq-D in the upper and lower six panels, respectively. The bar pattern speed and the amplitude are respectively shown in the upper and lower three panels of each group of panels as functions of cosmic time.

and then follow their evolution for a short period of time during which we can consider that the orientation of the disks do not change. We employ the output time-step of 10 Myr for these additional simulations.

In figure 5 we show the bar pattern speed, $\Omega_{\text{bar}} = \dot{\phi}_{\text{bar}}$, and the amplitude, A_2^{max} , as functions of time around $z = 1, 0.5$ and 0. Firstly, we find that the pattern speed of the bars slows down from $z = 1$ to 0 in both galaxies. The long-term behavior of Aq-C's bar is consistent with what we expect from the results of the idealized simulations, that is, the bar becomes stronger and longer as it rotates more slowly. Aq-D's bar however does not change its amplitude between $z \approx 1$ and 0.5 while its pattern speed decreases; and the bar amplitude becomes smaller from $z \approx 0.5$ to 0.

The pattern speed and the amplitude of Aq-C's bar display large short-term fluctuation at $z \approx 1$ and 0.5. Interestingly, the short-term behavior is similar to the long-term one, i.e. the bar gets stronger when the pattern speed decreases. This short-term fluctuation becomes smaller with time and almost vanishes at $z \approx 0$.

To see the short-term behaviors more closely, we now plot the pattern speed and the amplitude as functions of

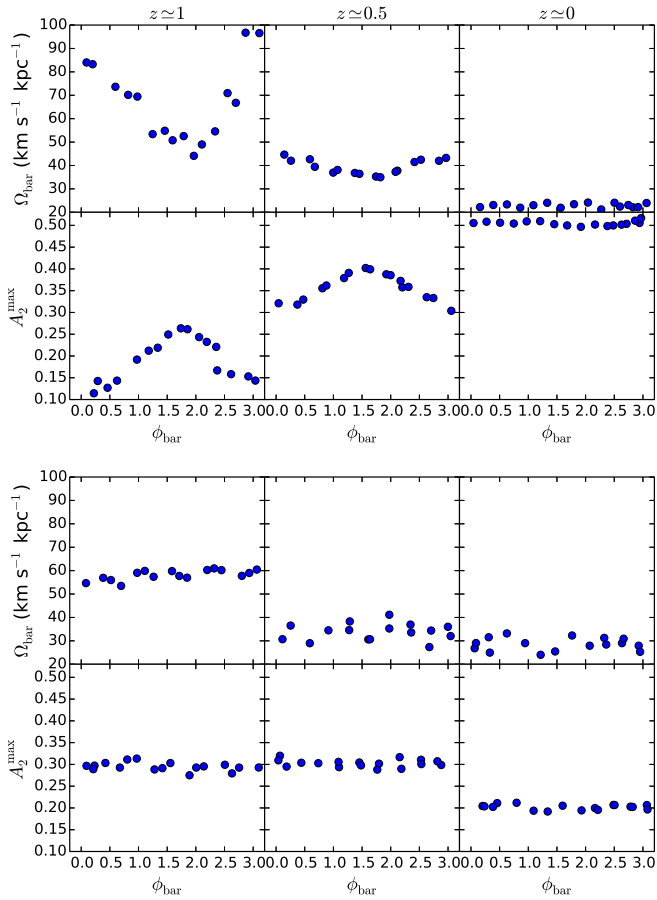


Fig. 6. Same as figure 5 but now as functions of the bar angle, ϕ_{bar} .

the bar angle in figure 6. We find that both the amplitude and the pattern speed vary with period of π when they show large short-term fluctuation (at $z \simeq 1$ and 0.5 in Aq-C). On the other hand, we do not observe such a periodicity for Aq-D’s bar.

3.4. Who obtains the angular momentum?

Since the bar pattern speed slows down from $z = 1$ to 0, we expect that the angular momentum of the bars is transferred to other components, such as outer disks or dark halos. In order to identify which component plays the most important role in spinning down the bars, we try to measure the torque from each component acting on the bars. Doing this is however not straightforward because defining particles that constitute the bar is not a simple task. It is also difficult to relate the measured torque to the change in the bar pattern speed even if we somehow define the particles that belong to the bar, since the angular momentum of the bar, $L_{\text{bar}} = I_{\text{bar}}\Omega_{\text{bar}}$, where I_{bar} is the moment of the inertia of the bar, is different from the total angular momentum of the particles that constitute the bar.

We therefore take a simpler approach. We define the bar region as a disk with the radius, r_{bar} , and the height $1 h^{-1}$ kpc and then compute the torques acting on the star

particles contained in this region. Since the z -component of the torque acting on an axisymmetric component is zero, the torque mainly operates on the bar as long as the bar is the most significant non-axisymmetric structure in the region. We have checked that we obtain qualitatively equivalent results when we calculate torques on the particles along the bar.

In figure 7, we show the z -component of the specific torque from the particles within the virial radius acting on the stars in the bar region as a function of the bar angle. We find that the torque from the dark halo dominates the total torque in Aq-C and it is negative on average; the torque from the dark matter spins down the stars in the bar region more strongly at higher redshift. In Aq-C, the torque from the dark matter shows the periodic change with a period of π . This behavior suggests that the torque is exerted by the anisotropic distribution of the dark matter.

Although the period with which the torque changes is the same as the period with which the pattern speed changes in Aq-C at $z \simeq 1$ and 0.5, the change in the angular momentum of the stars that constitute the bar is not directly reflected to the bar pattern speed. In the panels of $z \simeq 1$ and 0.5 for Aq-C, we indicate the bar angle where the bar pattern speed becomes the smallest. We find that, against the intuition, the torque takes the largest negative value where the bar pattern speed becomes the smallest. The pattern speed should be the smallest where the torque changes its sign from minus to plus if the angular momentum of the stars that constitute the bar were directly reflected to the pattern speed. Moreover, the pattern speed of Aq-C’s bar at $z \simeq 0$ is almost constant while the torque show the same level of variation as at $z \simeq 1$ and 0. This is a direct consequence of the fact that the bar angular momentum, $I_{\text{bar}}\Omega_{\text{bar}}$, is different physical quantity from the total angular momentum of the particles belonging to the bar as we mentioned earlier.

In Aq-D, the amplitude of the specific torque is much smaller than that in Aq-C. The long-term evolution of the bar pattern speed in Aq-D is thus much more moderate than in Aq-C. The torque is not always dominated by the contribution of the dark matter, for example the torque is dominated by that of the stars at $z \simeq 0.5$. This is consistent with the fact that the central density of the dark halo of Aq-D is much lower than that of Aq-C and thus there is less dark matter to absorb the angular momentum of the bar.

3.5. Interaction with the $m = 4$ Fourier mode

As shown in the previous subsection, the periodic change of the torque does not explain the periodic change of the bar pattern speed in Aq-C seen at high redshift. In this subsection, we investigate the second most significant Fourier mode, the $m = 4$ mode, and explore a possible interaction between the $m = 2$ and $m = 4$ Fourier modes.

In figure 8, we plot the amplitude and the phase profiles of the $m = 4$ Fourier mode. Since the phase of the $m = 4$ mode, $\phi_4(r)$, is defined between 0 and $\pi/2$, we also plot $\phi_4(r) + \pi/2$ to compare it with that of the $m = 2$

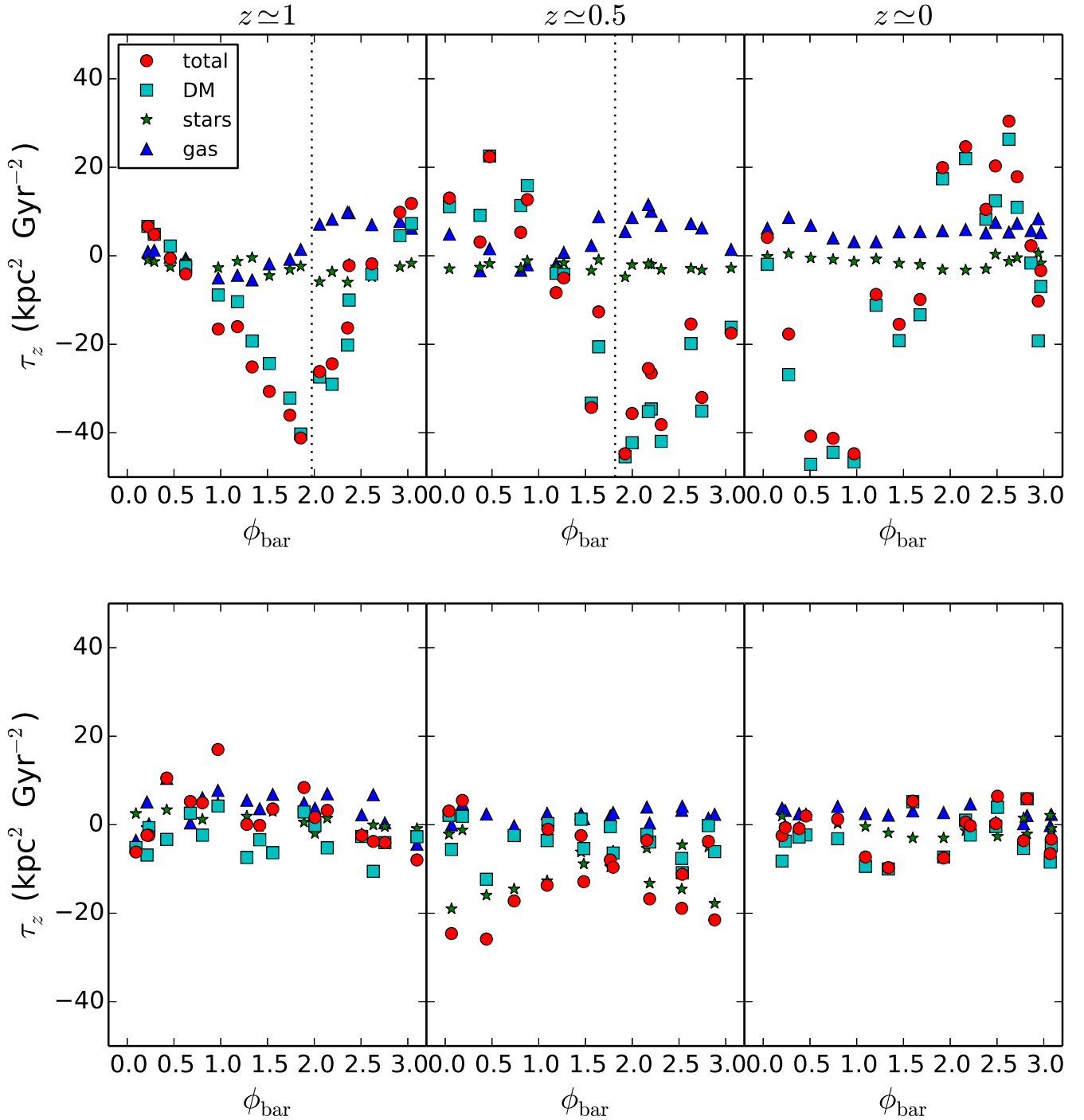


Fig. 7. The z -component of the specific gravitational torque acting on the stars in the bar regions at $z \simeq 1$, 0.5, and 0. The upper and lower panels show Aq-C and Aq-D, respectively. The red circles indicate torque from all the particles within virial radius, r_{vir} . The cyan squares, green stars, and blue diamonds respectively show the contributions of the dark matter, stars, and gas. The vertical dotted lines in the upper left and the upper middle panels indicate the bar angle at which the bar pattern speed is the smallest.

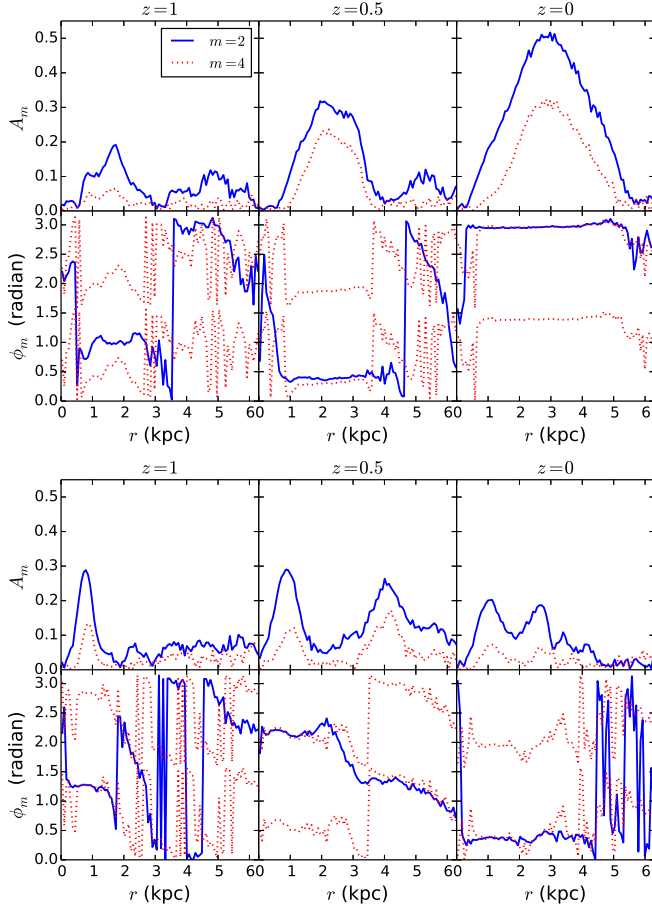


Fig. 8. The amplitude and phase profiles of the $m = 2$ and $m = 4$ modes. The upper and lower six panels show Aq-C and Aq-D, respectively. The blue solid and red dotted lines respectively represent the $m = 2$ and $m = 4$ modes. The amplitude and phase are shown in the upper and lower panels of each group of panels. From left to right, the results at $z = 1$, 0.5, and 0 are presented. For the phase, $\phi_4(r)$, we also plot $\phi_4(r) + \pi/2$ in order to compare it with the $m = 2$ mode.

mode, $\phi_2(r)$. Note that as Aq-C’s snapshot at $z \simeq 1$, we chose the one in which the misalignment between the two components is clearly visible.

We find that the amplitudes of the $m = 4$ components in both galaxies are in fact significant and their spatial extent is comparable with the $m = 2$ components, the bars. In Aq-C, the $m = 2$ component is largely misaligned with the $m = 4$ component at $z = 1$ and is slightly misaligned at $z = 0.5$. At $z = 0$ the two modes are perfectly aligned with each other. On the other hand, the two modes are always aligned in Aq-D. We thus speculate that a bar shows rapid short-term fluctuation in its pattern speed when it is misaligned with the $m = 4$ component.

Next, we explore the relation between the pattern speed and amplitude of the $m = 2$ and $m = 4$ components. To calculate the pattern speed of the $m = 4$ component, we define A_4^{\max} and r_4^{\max} by exactly the same way as we defined A_2^{\max} and r_2^{\max} and then we define the phase of the $m = 4$ component as $\phi_4(r_4^{\max})$.

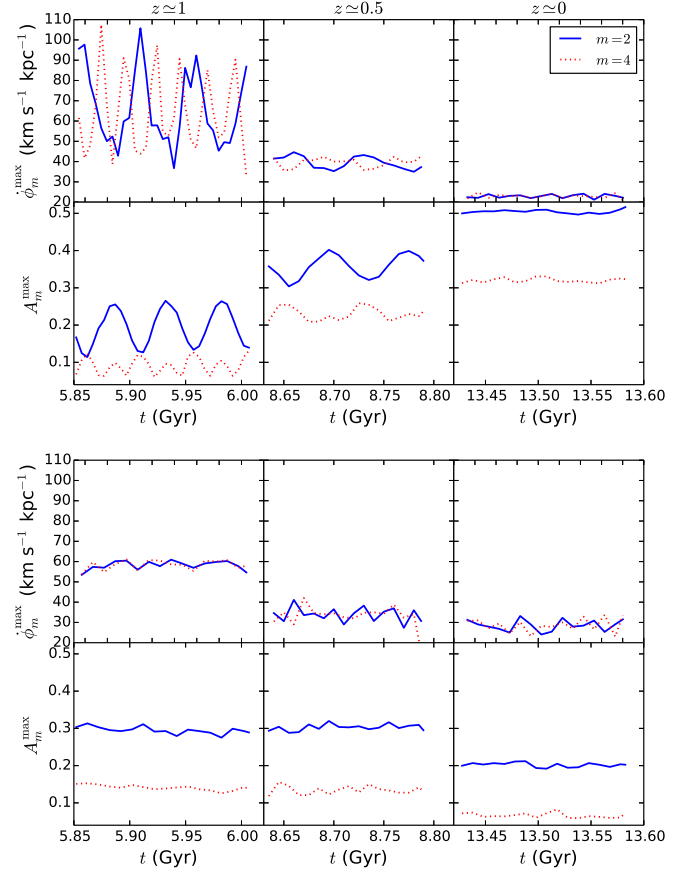


Fig. 9. Same as figure 5 but we now show the pattern speed and amplitude of the $m = 4$ components as well. The $m = 2$ and $m = 4$ components are respectively represented by the blue solid and red dotted lines.

In figure 9, we show the pattern speed of the $m = 2$ component, $\Omega_{\text{bar}} \equiv \dot{\phi}_{\text{bar}}$, and the $m = 4$ component, $\dot{\phi}_4(r_4^{\max})$. We find that the pattern speed of the $m = 4$ component also shows large and periodic time variation at $z \simeq 1$ in Aq-C. This time variation becomes much smaller at $z \simeq 0.5$ at which the misalignment between the two modes is small (see figure 8). Once the phases of the two components are perfectly aligned with each other, the pattern speed of the both components becomes almost constant and of course the two components have the same pattern speed.

The amplitude of the $m = 4$ component also varies with the same period as the pattern speed. As for the $m = 2$ component, the amplitude becomes large when the pattern speed is small and vice versa. The frequency of the oscillation of the pattern speed of the $m = 4$ component is clearly higher than that of the $m = 2$ component. We find that the period of the oscillation of the pattern speed and the amplitude of the $m = 4$ component is $\pi/2$ if we plot these variables as functions of the phase, $\phi_4(r_4^{\max})$.

As we have shown, the $m = 2$ and $m = 4$ components in Aq-D are always aligned with each other. In this case, the pattern speed and the amplitude of both the $m = 2$ and $m = 4$ components do not show the large short-term fluctuation, which is seen in Aq-C at $z \simeq 1$ and 0.5. We

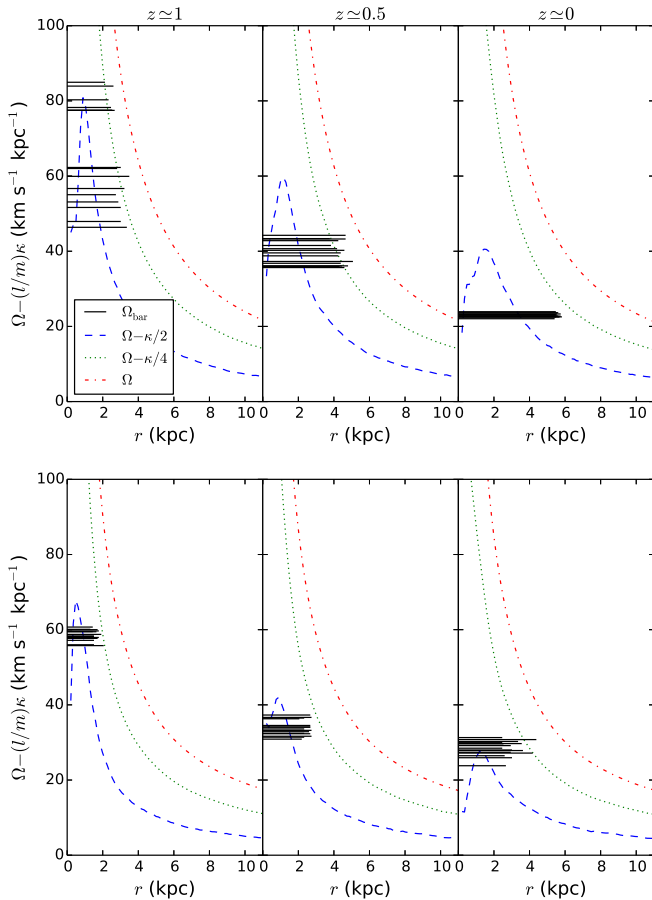


Fig. 10. Behavior of $\Omega - \kappa/2$, $\Omega - \kappa/4$ and Ω at $z = 1, 0.5$, and 0 . The blue dashed, green dotted, and red dot-dashed lines respectively represent $\Omega - \kappa/2$, $\Omega - \kappa/4$, and Ω . The upper and lower panels indicate Aq-C and Aq-D, respectively, and redshifts are 1, 0.5, and 0 from left to right. We show the bar pattern speed around these redshifts by the horizontal black solid lines, whose lengths correspond to the bar lengths.

thus conclude that the pattern speed of the bar oscillates if its phase is misaligned with the phase of the $m = 4$ component in the same region.

3.6. Resonances and the bar length

Finally we investigate the resonance structure of the simulated galaxies. In figure 10 we show the behaviors of $\Omega - \kappa/2$, $\Omega - \kappa/4$, and Ω as functions of radius, where Ω is the angular frequency of a circular orbit and κ is the radial angular frequency. Each $\Omega - \kappa/2$ curve has a peak and therefore these galaxies have double inner Lindblad resonances (ILRs) if the bar pattern speed is smaller than the peak value. The peak values decrease with time since the central density of the galaxies decrease with time due to the stellar evolution and the feedback (see figure 1).

The density structure does not change on the short time-scale during which we measure the pattern speed of the bars around $z = 1, 0.5$, and 0 . We show the bar pattern speed and the bar length measured around these redshifts by the horizontal lines. From the behavior of the bar pat-

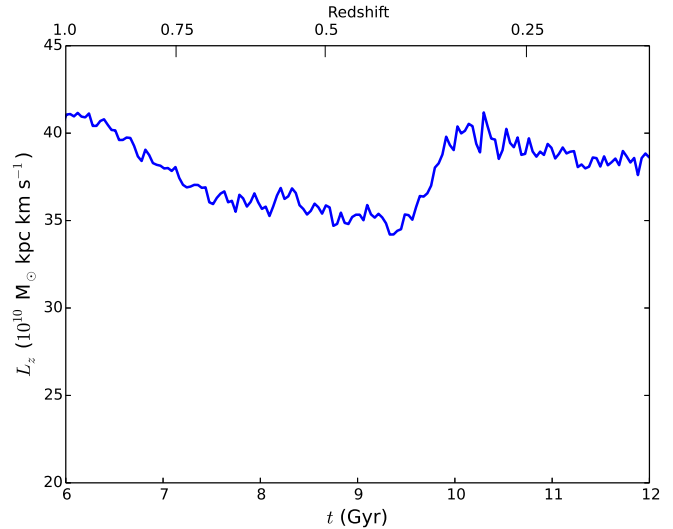


Fig. 11. Angular momentum evolution of the stellar component in the bar region in Aq-D. The line indicates the total angular momentum of the stellar disk of the radius, $r_{\text{bar}} = 1.68$ kpc, and the height, $1 h^{-1}$ kpc, in Aq-D.

tern speed and the amplitude in Aq-C around $z = 1$ and 0.5 , we speculate that the smaller the pattern speed is, the larger the amplitude is if $\Omega - \kappa/2$ curve is fixed.

On the long time-scale, $\Omega - \kappa/2$ curve is lowered as shown in figure 10. In Aq-C, the bar pattern speed strongly decreases from $z = 1$ to 0 . As a result, the bar amplitude becomes larger with time (figure 4). In Aq-D, the slow down rate of the bar pattern speed is much lower than that in Aq-C. Consequently, the peak value of $\Omega - \kappa/2$ value decreases as fast as or faster than the bar pattern speed. The bar amplitude in this case does not change much or becomes smaller as shown in figure 4. At $z \simeq 0$, there is no $2(\Omega - \Omega_{\text{bar}}) = \kappa$ resonances in many cases. As a result, the bar amplitude at $z = 0$ is smaller than that at $z = 0.5$. We will discuss the sharp decline in the amplitude of Aq-D's bar at $t \sim 9.8$ Gyr shown in figure 4 in the next section.

The bar lengths lie between the ILRs and the corotation radii as long as the ILRs exist. Interestingly enough, the bar lengths are around $4(\Omega - \Omega_{\text{bar}}) = \kappa$ resonances in both galaxies at any redshifts. It might be just a coincidence but there might be something more behind this. As shown in figure 8, there is the $m = 4$ component whose phase coincides with the bar angle and whose spatial extent is comparable to the bar length. The interaction between two modes may set the bar length.

4. Discussion and conclusions

We have investigated the cosmological evolution of bars by utilizing the two Milky Way-mass galaxies formed in the fully self-consistent simulations of the galaxy formation by Okamoto (2013). The evolution qualitatively agrees with what is expected from idealized simulations, that is, the bar in the galaxy having more centrally

concentrated mass distribution exhibit stronger evolution than the other (Combes & Elmegreen 1993; Athanassoula 2003). The bar in Aq-C receives the large negative torque from the dark matter and is significantly slowed down its rotation from $z = 1$ to 0. As the bar pattern speed decreases, the bar becomes stronger and longer. On the other hand, the torque acting on Aq-D's bar is much weaker by lacking materials that absorb the angular momentum of the bar.

The bars however show several behaviors that are usually not seen in idealized simulations. The pattern speed of Aq-C's bar violently oscillates at $z \simeq 1$. The oscillation becomes smaller at $z \simeq 0.5$ and disappears at $z \simeq 0$. Interestingly, the period of the oscillation as a function of the bar angle is π . The amplitude of the bar also shows the short-term fluctuation. When the bar rotates slower, it becomes stronger and vice versa. This short-term behavior is consistent with the long-term behavior in Aq-C, i.e. the slower the bar rotation is, the larger its amplitude is.

The evolution of the bar in Aq-D seems to contradict this scenario. While the pattern speed of the bar decreases with time, its amplitude does not increase from $z = 1$ to 0.5 and even decreases from $z = 0.5$ to 0. We speculate that this is because $\Omega - \kappa/2$ curve is lowered with time (figure 10) due to the decreasing central density with time (figure 1), which is most likely caused by the mass loss and feedback from the stellar populations. The inclusion of the timed release of mass and energy from stellar populations is one of the biggest differences between our cosmological simulations and other idealized simulations. Thanks to the effective angular momentum transfer from the bar to the dark matter in Aq-C, the bar pattern speed drops faster than $\Omega - \kappa/2$ curve, and thus the bar becomes stronger. On the other hand, the slow down rate of Aq-D's bar is as low as the decreasing rate of the peak value of $\Omega - \kappa/2$ curve.

If this interpretation is correct, there must be an abrupt change either in the central density structure or in the bar pattern speed at $t \sim 9.8$ Gyr in Aq-D, at which the amplitude of the bar suddenly drops. We have confirmed that the density structure and hence $\Omega - m\kappa/l$ curves do not show such abrupt changes at this epoch. Unfortunately, we cannot measure the pattern speed around this epoch because of the coarse time-step used to output the simulation snapshots. Instead, we measure the angular momentum of the stars in the bar region as a proxy for the pattern speed. Although the angular momentum of the stars is not immediately reflected to the bar pattern speed as we have shown in section 3.4, it does nevertheless correlate with the pattern speed (Athanassoula 2003).

Since the bar length is more or less constant around $t \sim 9.8$ Gyr if we ignore the outer component (see figure 4), we investigate the evolution of the angular momentum of the stars in the disk of radius, $r_{\text{bar}} = 1.68$ kpc and the height, $1 h^{-1}$ kpc, which is depicted in figure 11. We find that the angular momentum indeed rapidly increases when the amplitude sharply decreases. The angular momentum is most presumably brought by the sinking stellar

clumps seen in the panel for $z = 0.5$ of figure 3. Okamoto (2013) has shown that a non-negligible amount of mass is added to Aq-D's bulge by these clumps. Note that we obtain a qualitatively equivalent result if we plot the specific angular momentum instead of the angular momentum in figure 11. This result strongly support the idea that the bar amplitude is determined by the relation between the pattern speed and $\Omega - \kappa/2$ curve.

The significant fluctuation in the bar pattern speed and the bar amplitude is observed only when the $m = 2$ component is misaligned with the $m = 4$ component. The fluctuation becomes smaller as the two components get aligned with each other. The $m = 4$ components have the comparable spacial size to the $m = 2$ components in both galaxies. Interestingly, the bar lengths seem to be determined by $4(\Omega - \Omega_{\text{bar}}) = \kappa$ resonances. This might be just a coincidence because this resonance always lie between the ILR and the corotation radius, but might be the result from the interaction between the two modes. Observationally, NGC 253 seems to have a bar whose length coincides with $4(\Omega - \Omega_{\text{bar}}) = \kappa$ resonance (Sorai et al. 2000).

In summary, using the high-resolution cosmological simulations of disk galaxies, we show that the bar evolution is much more complicated than that obtained by idealized simulations of the isolated galaxies. The biggest difference from the idealized simulations is the inclusion of timed release of mass and energy from stellar populations, which significantly alters the central density structure and hence the resonance structure with time. We cannot identify what originates the misalignment between the bar and the $m = 4$ component, which causes the large fluctuation in the pattern speed and amplitude of the bar. Our sample is too small to derive any robust conclusions on this issue and thus we leave it for future research.

We would like to thank Masafumi Noguchi and Junich Baba for helpful discussion. Numerical simulations were carried out with Cray XC30 in CfCA at NAOJ and T2K-Tsukuba in Center for Computational Sciences at University of Tsukuba. TO acknowledges the financial support of Japan Society for the Promotion of Science (JSPS) Grant-in-Aid for Young Scientists (B: 24740112).

References

- Athanassoula, E. 2003, MNRAS, 341, 1179
- . 2005, MNRAS, 358, 1477
- . 2008, MNRAS, 390, L69
- Barazza, F. D., Jogee, S., & Marinova, I. 2008, ApJ, 675, 1194
- Berentzen, I., Athanassoula, E., Heller, C. H., & Fricke, K. J. 2004, MNRAS, 347, 220
- Combes, F., Debbasch, F., Friedli, D., & Pfenniger, D. 1990, A&A, 233, 82
- Combes, F., & Elmegreen, B. G. 1993, A&A, 271, 391
- Combes, F., & Sanders, R. H. 1981, A&A, 96, 164
- Curir, A., Mazzei, P., & Murante, G. 2006, A&A, 447, 453
- Debattista, V. P., Carollo, C. M., Mayer, L., & Moore, B. 2004, ApJL, 604, L93
- Debattista, V. P., & Sellwood, J. A. 2000, ApJ, 543, 704

- Duffy, A. R., Schaye, J., Kay, S. T., et al. 2010, MNRAS, 405, 2161
- Efstathiou, G., Lake, G., & Negroponte, J. 1982, MNRAS, 199, 1069
- Eke, V. R., Cole, S., & Frenk, C. S. 1996, MNRAS, 282, 263
- Eskridge, P. B., Frogel, J. A., Pogge, R. W., et al. 2000, AJ, 119, 536
- Frenk, C. S., White, S. D. M., Davis, M., & Efstathiou, G. 1988, ApJ, 327, 507
- Governato, F., Zolotov, A., Pontzen, A., et al. 2012, MNRAS, 422, 1231
- Guedes, J., Callegari, S., Madau, P., & Mayer, L. 2011, ApJ, 742, 76
- Heller, C. H., Shlosman, I., & Athanassoula, E. 2007, ApJL, 657, L65
- Jing, Y. P., & Suto, Y. 2002, ApJ, 574, 538
- Klypin, A., Kravtsov, A. V., Valenzuela, O., & Prada, F. 1999, ApJ, 522, 82
- Kraljic, K., Bournaud, F., & Martig, M. 2012, ApJ, 757, 60
- Marinacci, F., Pakmor, R., & Springel, V. 2014, MNRAS, 437, 1750
- Martinez-Valpuesta, I., Shlosman, I., & Heller, C. 2006, ApJ, 637, 214
- Miwa, T., & Noguchi, M. 1998, ApJ, 499, 149
- Moore, B., Ghigna, S., Governato, F., et al. 1999, ApJL, 524, L19
- Okamoto, T. 2013, MNRAS, 428, 718
- Okamoto, T., Eke, V. R., Frenk, C. S., & Jenkins, A. 2005, MNRAS, 363, 1299
- Okamoto, T., Frenk, C. S., Jenkins, A., & Theuns, T. 2010, MNRAS, 406, 208
- Okamoto, T., Gao, L., & Theuns, T. 2008, MNRAS, 390, 920
- Okamoto, T., Shimizu, I., & Yoshida, N. 2014, PASJ, 66, 70
- Pfenniger, D., & Norman, C. 1990, ApJ, 363, 391
- Romano-Díaz, E., Shlosman, I., Heller, C., & Hoffman, Y. 2008, ApJL, 687, L13
- Scannapieco, C., & Athanassoula, E. 2012, MNRAS, 425, L10
- Scannapieco, C., Wadepuhl, M., Parry, O. H., et al. 2012, MNRAS, 423, 1726
- Sheth, K., Elmegreen, D. M., Elmegreen, B. G., et al. 2008, ApJ, 675, 1141
- Sorai, K., Nakai, N., Kuno, N., Nishiyama, K., & Hasegawa, T. 2000, PASJ, 52, 785
- Springel, V., Wang, J., Vogelsberger, M., et al. 2008, MNRAS, 391, 1685
- Stinson, G. S., Brook, C., Macciò, A. V., et al. 2013, MNRAS, 428, 129
- Weinberg, M. D. 1985, MNRAS, 213, 451